RESEARCH ARTICLE

Check for updates

Antisolvent solubilization achieves simultaneous passivation of shallow and deep defects in perovskite solar cells†

Chu Zhang,[a] Chunying Ma,[a] Shennan Chen[a] and Tingli Ma [iD] *[a,b]

Resolving the inherent defects at the interfaces and grain boundaries of perovskite films is crucial for achieving highly efficient and stable perovskite solar cells (PSCs). This study introduces an antisolvent solubilization (AS) approach to enhance the solubilization of the bulk organic ammonium salt 2-Thiophenemethylammonium Iodide (ThMAI), which has limited solubility in low-polarity antisolvents. The results demonstrated that the AS approach could effectively passivate both shallow and deep defects in organic–inorganic hybrid perovskites (OIHPs). Furthermore, the ThMAI prepared using the AS method could react with excess PbI$_2$ and facilitate the crystallization of the OIHPs, thereby improving light absorption, suppressing non-radiative recombination, and enhancing carrier extraction. As a result, PSCs prepared by using the AS method achieved a power conversion efficiency (PCE) of 23.69%, representing a 10% PCE improvement compared to normal devices. PSCs based on the AS method also demonstrated significantly improved heat and humidity stability.

1. Introduction

As one of the most promising photoelectric materials, organic–inorganic hybrid perovskites (OIHPs) and their derivatives have garnered significant attention.[1–4] The corresponding devices, known as perovskite solar cells (PSCs), have achieved certified power conversion efficiencies (PCE) of 26.1%.[5] However, the inherent defects in OIHPs, including shallow and deep defects resulting from the preparation process and crystallinity, pose notable challenges to the photovoltaic performance and stability of PSCs. These defects contribute to an increase in non-radiative recombination and a decrease in the PCE of PSCs.[6–8]

To minimize the detrimental effects of defects in perovskite materials, researchers have employed various strategies, such as compositional engineering,[9] dopant engineering,[10,11] passivation,[12,13] and the formation of graded junctions.[14] Passivation, in particular, is an essential optimization approach that can target the bulk, surface, and grain boundaries of the material. It effectively reduces non-radiative

recombination, improves charge carrier transport through band alignment, and enhances stability by utilizing hydrophobic passivation materials.[15–17] Defects have been found to be abundant at the surface and grain boundaries, with concentrations 2–4 orders of magnitude higher than those in the bulk.[18] Consequently, passivating defects at the surface and grain boundaries has emerged as the most straightforward and effective method. Additives such as Lewis acids[19] or bases,[20] as well as zwitterion molecules,[21] are typically incorporated into the precursor to passivate deep defects at grain boundaries. For the passivation of shallow surface defects, ultrathin layers of polymers,[22] inorganic molecules,[23] layered perovskites,[24] and small organic amines[25] have been employed. However, there are limited reports on simultaneously passivating both shallow surface and deep defects.

In this paper, we investigated the use of an antisolvent solubilization (AS) approach to improve the solubility of bulk organic ammonium salts, which typically have low solubility in antisolvents with low polarity. Results demonstrated that when antisolvent solubilization was employed, the bulk organic ammonium salt 2-ThiophenemethylammoniumIodide (ThMAI) could react with excess PbI$_2$ and facilitate the crystallization of OIHPs during the crystallization process. This approach induced the simultaneous passivation of defects at both the shallow surface and deep grain boundaries, leading to improve PCE and stability of the OIHPs material.

[a]College of Materials and Chemistry, China Jiliang University, Hangzhou, 310018, P. R. China. E-mail: matingli123@cjlu.edu.cn
[b]Graduate School of Life Science and Systems Engineering, Kyushu Institute of Technology, Kitakyushu, Fukuoka 808-0196, Japan

2. Results and discussion

A common organic solvent, isopropyl alcohol (IPA), was used to solubilize the bulk organic ammonium salts (ThMAI) in the antisolvent (chlorobenzene). Since the OIHPs precursor has not crystallized during the antisolvent drip, the bulk organic ammonium salts (ThMAI) would penetrate into OIHPs layer, as cross-sectional energy dispersive spectrometer (EDS) mapping shown in Fig. 1a and b. Compared with the OIHPs prepared without AS method, the S element appeared at the shallow surface and deep domain in OIHPs prepared by AS method. It indicated that the bulk organic ammonium salts (ThMAI) had penetrated to the surface and grain boundaries of OIHPs. X-ray Diffraction (XRD), as shown in Fig. 1c, demonstrated that the AS method facilitated the crystallization of OIHPs, where two dominant diffraction peaks at 14.1° and 28.4° are enhanced. It could be confirmed by scanning electron microscope (SEM) in Fig. 1d and e. Compared with the OIHPs prepared without AS method, the average grain size of OIHPs prepared with AS method was increased about 70 nm (from 195 nm to 265 nm, as shown in Table S1†). In addition, the diffraction peak at 12.7° indicative of the existence of the excess PbI_2 was lower in OIHPs prepared with AS method, which indicated that the ThMAI could react with the excess PbI_2.[26] The enlarged grain size and reduced PbI_2 defects in OIHPs prepared with AS method led to better light absorption and suppressed recombination (Fig. S1†). The lower PL inten-sity indicated a faster charge extraction between the modified OIHPs and carrier transport layer, and the better crystallization would induce enhanced light absorption.

In order to demonstrate the passivation effect of AS method, space charge limited current (SCLC) of hole transport layer (HTL) only devices (FTO/PEDOT:PSS/OIHPs/spiro-MeOTAD/Au) has been carried out. The curves was divided into three regions. In the range of low voltage, the current increase linearly with the increase of voltage, representing an ohmic regime (the slope is 1, as green line shown in Fig. 1f). The second section is the trap-filled limit regime (yellow line). The third section, namely the trap-free regime (blue line). According to the equation $N_t = \frac{2V_{TFL}\varepsilon_0\varepsilon_r}{qL^2}$, the trap state density N_t can be obtained, where V_{TFL} is the trap-filled limit voltage, L is the thickness of the perovskite film, ε_r is the relative dielectric constant of perovskite material, and ε_0 is the vacuum permittivity. The calculation of the trap state density demonstrated that there was less trap state in AS modified HTL only devices (5.91×10^{17} cm^{-3}), compared with devices without AS modified (6.79×10^{17} cm^{-3}), as shown in Fig. 1f.[27] The lower trap state density came from two aspects: larger OIHPs grains could effectively reduce the trap state density in the bulk; the ThMAI treatment in AS method could passivate defects of both the surface and grain boundaries. In addition, we compared the differences between AS method and conventional post-treatment method for the passivation of OIHPs films. Compared with AS method, the post-treatment with
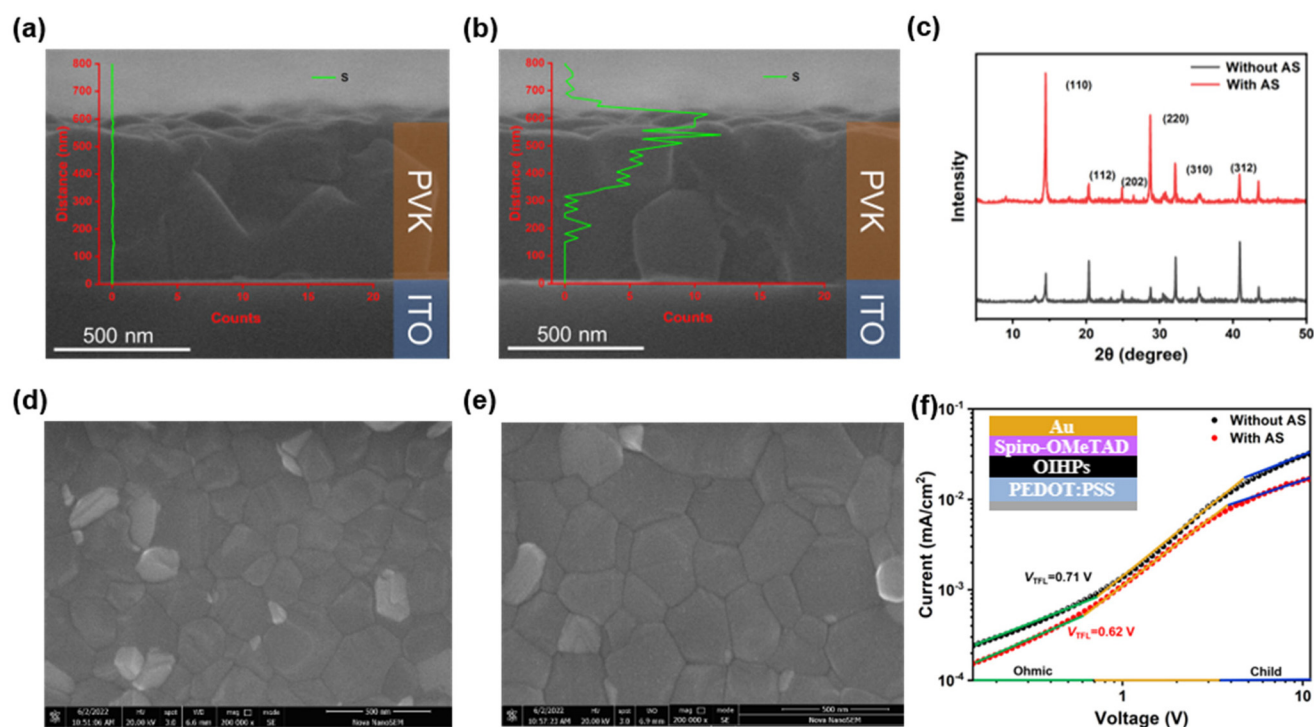

Fig. 1   Cross-section images and EDS mapping of OIHPs films without (a) and with (b) AS method; (c) XRD patterns of OIHPs films without and with AS method; (d) and (e) were the top SEM of the OIHPs prepared without and with AS method; (f) SCLC curves of pure hole transport devices based on OIHPs prepared without and with AS method.

This journal is © the Partner Organisations 2024

Inorg. Chem. Front., 2024, **11**, 1472–1478 | **1473**

ThMAI could only passivate the surficial defects, where the ThMAI only left on the surface of the OIHPs, as shown in Fig. S2.†

The evaluation of photovoltaic performance of PSCs based on OIHPs prepared without and with AS method were shown in Fig. 2a, where the amount of ThMAI has been optimized, as shown in Fig. S3.† Results demonstrated that 23.69% PCE of champion device based on AS method was obtained, which was much larger than that of compared devices (21.53%), the corresponding detail parameter was shown in Table S2 and Fig. S4.† The PSCs prepared with AS method showed much smaller hysteresis. Fig. 2b showed incident photon-to-electron conversion efficiency (IPCE) spectra of the corresponding devices. The integrated current densities estimated from the IPCE spectra are in good agreement with the J_{sc} values obtained from the J–V curves. The stabilized power outputs (SPOs) of PSCs prepared without and with AS method are 20.12% and 22.61%, respectively (Fig. 1c), which are consistent with the J–V measurements. The reproducibility of the device performance was also evaluated by characterizing about 26 cells. The frequency histogram of the PCE parameters of these devices (Fig. 1d) indicated that the AS method had good reproducibility.

To clarify the mechanism of device performance enhancement, we conducted a series of carrier transport performance tests on the two devices, as shown in Fig. 3. Nyquist plots of the PSCs prepared without and with AS method were shown in Fig. 3a. Two arcs could be seen in each curve in Nyquist's diagram. The arcs in the high frequency region were closely related to charge transfer resistance (R_{tr}), while the arcs in the low frequency region were related to recombination resistance (R_{rec}).[28] The electrochemical impedance spectroscopy (EIS) fitting parameters were summarized in Table S3.† Compared with PSCs prepared without AS method, R_{tr} of PSCs prepared with AS method decreased and R_{rec} increased, indicating that PSCs prepared with AS method were more conducive to charge transfer and could effectively inhibit non-radiative recombination. In order to understand the charge transfer dynamics of PSCs prepared by different methods, transient photovoltage (TPV) and transient photocurrent (TPC) decay measurements were carried out to determine the charge carrier kinetics in different devices. As presented in Fig. 3b, the photovoltage decay time of PSCs prepared with AS method (67.4 μs) was longer than that of PSCs prepared without AS method (51.6 μs), which was mainly due to the reduction of defects in OIHPs film after ThMAI modification. And the suppression of
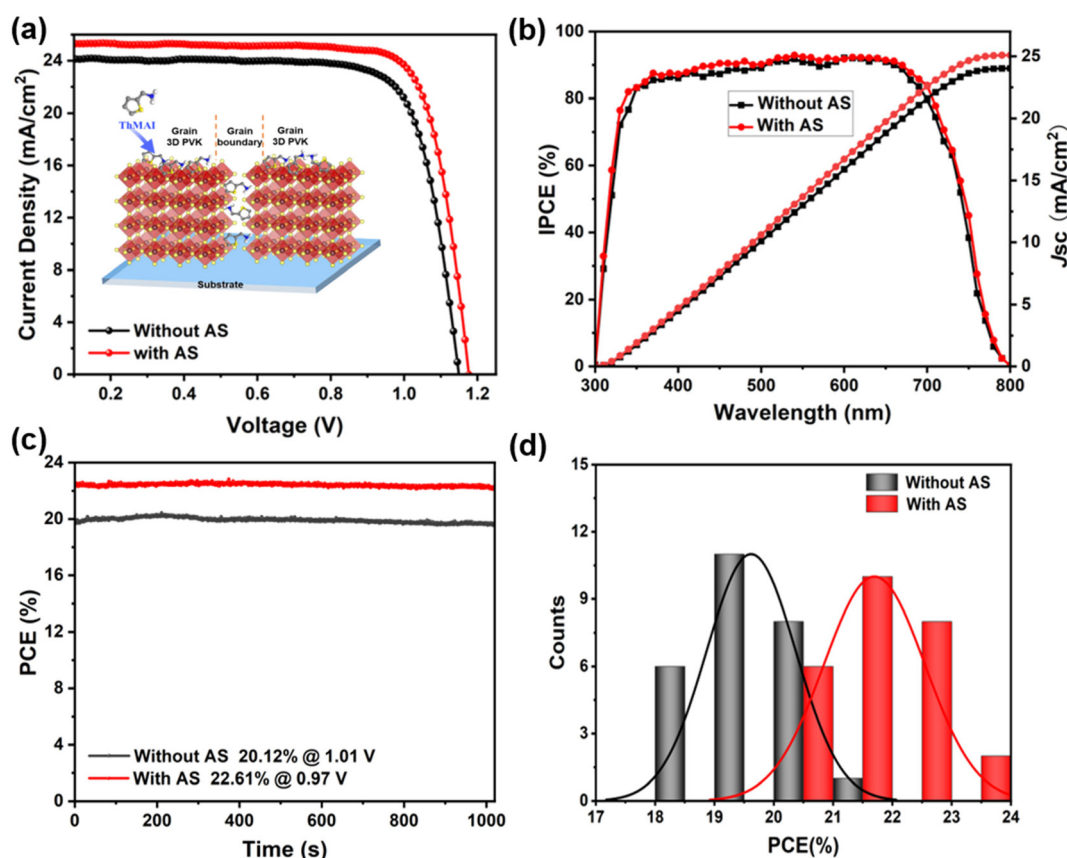

Fig. 2 (a) J–V curves (reverse scan) of champion devices fabricated without and with AS methods; (b) IPCE curves of champion devices fabricated without and with AS methods; (c) SPOs of different PSCs was operated at the maximum power point under simulated AM 1.5G sunlight of 100 mW cm^{-2}; (d) reproducibility of 26 devices fabricated using different methods.

1474 | *Inorg. Chem. Front.*, 2024, **11**, 1472–1478

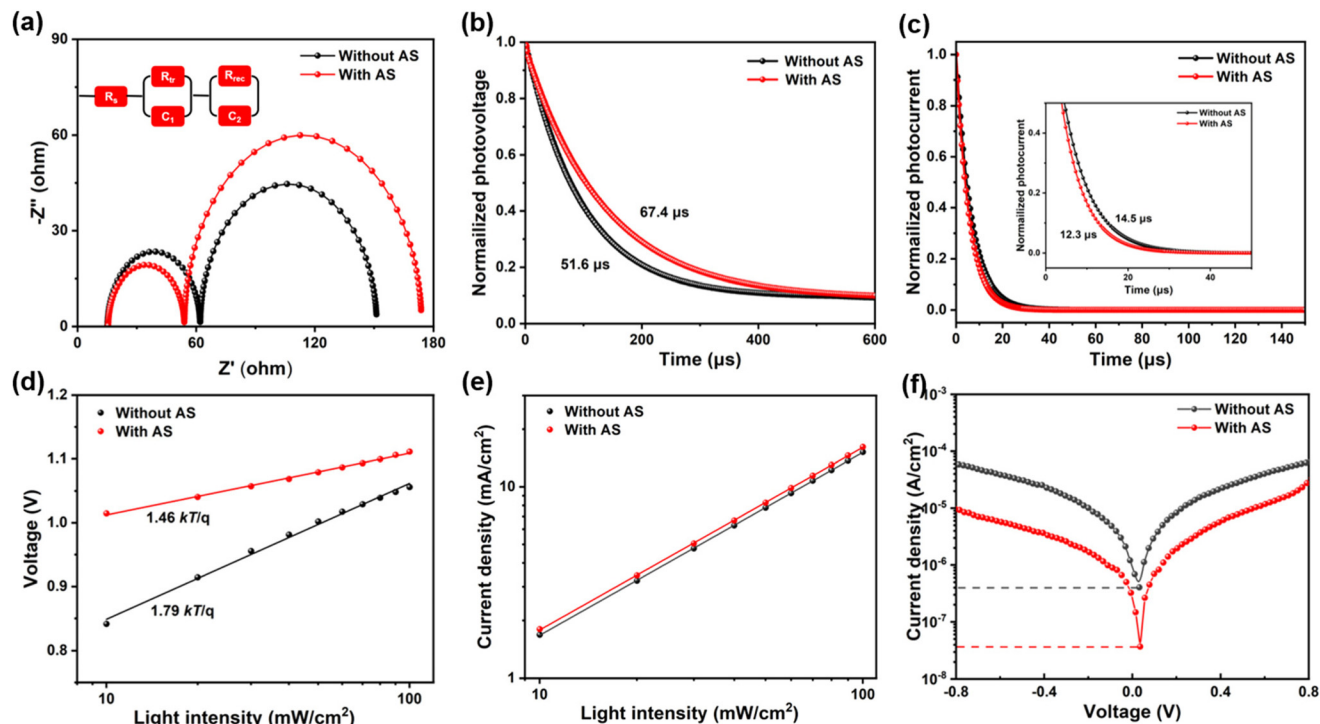This journal is © the Partner Organisations 2024

Fig. 3 (a) Nyquist plot of PSCs fabricated without and with AS methods measured in the dark at $V \approx V_{oc}$; (b) TPV and (c) TPC decay curves of PSCs fabricated without and with AS methods; (d) IMVS and (e) IMPS of PSCs fabricated without and with AS methods; (f) dark current curves of PSCs fabricated without and with AS methods.

non-radiative recombination eventually lead to the increase of V_{oc} and FF. The TPC measurements, as shown in Fig. 3c, showed that the faster photocurrent decay rate of PSCs prepared with AS method. It implied that its charge transport efficiency was higher than that of PSCs prepared without AS method, which would effectively inhibit the charge accumulation at the OIHPs/HTL interface, resulting in the enhanced J_{sc}.

Furthermore, we tested intensity-modulated photovoltage spectroscopy (IMVS) and intensity-modulated photocurrent spectroscopy (IMPS), which compared the dependence of V_{oc} and J_{sc} on light intensity for different PSCs. Typically, if there is less Shockley–Read–Hall (SRH) recombination, the slope of V_{oc} *versus* light intensity will decrease.[29] As shown in Fig. 3d, the PSCs prepared with AS method had a smaller slope of $1.46kT/q$ compared to PSCs prepared without AS method
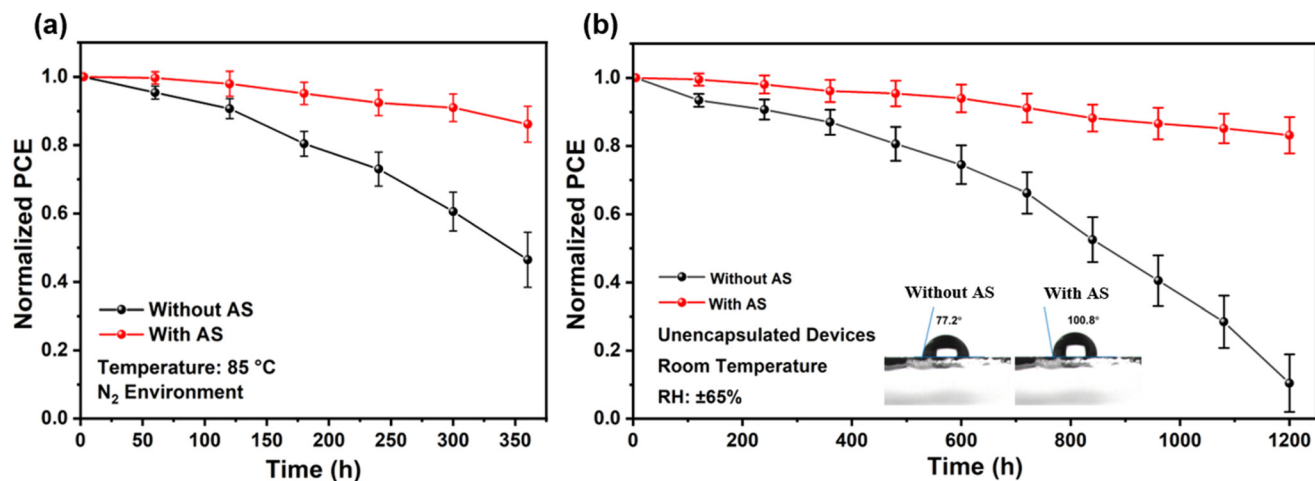

Fig. 4 Long-term stability of PSCs prepared without and with AS method at different ambient atmosphere without any encapsulation (a) 85 °C in N₂ environment; (b) 25 °C, 65%RH (the insert image showed the contact angle test of devices without and with AS method).

This journal is © the Partner Organisations 2024

Inorg. Chem. Front., 2024, **11**, 1472–1478 | **1475**

(slope of $1.79kT/q$). A lower slope meant fewer defect-assisted recombination centers, which further demonstrated that ThMAI modification could effectively passivate grain boundaries and interfacial defects. In addition, the PSCs prepared with AS method had a higher J_{sc} under the same lighting conditions, as shown in Fig. 3e. This indicated that more free carriers were transferred and collected before recombination in PSCs prepared with AS method.[30] Dark state saturation current density obtained through the dark J–V curve showed that the saturation current density of PSCs prepared with AS method under dark conditions was estimated to be 3.65×10^{-8} mA cm^{-2}, which was found to be one order of magnitude lower than the device prepared without AS method (4.05×10^{-7} mA cm^{-2}), illustrating the PSCs prepared with AS method exhibited lower current leakage than the control devices, as shown in Fig. 3f.

Stability comparison of PSCs based on different methods is carried out at high temperature (85 °C, N_2 environment), as shown in Fig. 4a. Error bars represent the standard deviation calculated from five devices prepared under the same conditions. The results showed that the efficiency of the PSCs prepared without AS method was less than 50% of the initial efficiency after 350 h of storage, while the PSCs prepared with AS method could maintain more than 80% of the initial efficiency. In high humidity atmosphere (25 °C, 65%RH), the PSCs prepared with AS method could keep 82% of their initial PCE for 1200 h, as shown in Fig. 4b. In order to investigate the reason of PSCs prepared with AS method possessed better heat and humidity stability, X-ray Photoelectron Spectroscopy (XPS) test has been carried out. Results showed that the peak of Pb $4f_{5/2}$ and Pb $4f_{7/2}$ were shifted toward lower binding energies in the ThMAI modified OIHPs film (Fig. S5†), which indicated that S in ThMAI had a strong interaction with Pb, which better stabilized the lattice of OIHPs. Contact angle measurements demonstrated that the OIHPs film fabricated using the ThMAI modification had a better hydrophobic property than OIHPs prepared without AS method, as shown in Fig. 4b. This prevented moisture from eroding the OIHPs crystals. Therefore, PSCs prepared with AS method showed stronger stability.

3. Conclusions

In summary, a bulk organic ammonium salt (ThMAI) has been solubilized by an AS method, which could simultaneously passivate the shallow and deep defects in OIHPs. Results demonstrated that the ThMAI modification in AS method could not only passivate the defects, but also be conducive to the crystallization of OIHPs. After deeply understand photophysics, PSCs prepared with AS method showed suppressed non-radiative recombination, reduced trap state density, and effective carrier's extraction, leading to 10% improvement in PCE (23.69%). PSCs based on AS method also demonstrated much better heat and humidity stability due to the interaction of ThMAI and Pb^{2+} and hydrophobic property of the bulk organic

ammonium salt. This study may extend the possibilities of passivation method in PSCs and induce high efficiency.

4. Experiments

Materials

Fluorine-doped tin oxide (FTO, ~15 Ω □$^{-1}$) conductive glass was purchased from Yingkou OPV Tech New Energy Co., Ltd. Tetrabutyl titanate (97%), diethanolamine (99.5%), dimethyl sulfoxide (DMSO, 99.9%), N,N-dimethylformamide (DMF, 99.8%) and chlorobenzene (99.8%) were all purchased from Sigma-Aldrich, respectively. Thiodiglycolic acid (TDGA, 98%) and concentrated hydrochloric acid (HCl, 25%) were purchased from J&K Chemical Technology. Urea (99.999%) and SnCl$_2$·H$_2$O (99.99%) were purchased from Aladdin Biochemical Technology Co., Ltd. CsI (99.9%), MABr (99.5%), PbBr$_2$ (99.99%), FAI (99.5%) and PbI$_2$ (99.99%) were purchased from Xi'an Polymer Light Technology Corp.

Device fabrication

FTO/CBD SnO$_2$ substrate and OIHPs precursor. Ultrasonic cleaning of FTO conductive substrate (2 cm × 2 cm) was carried out for 15 min according to the sequence of deionized water, acetone, and absolute alcohol, respectively. After cleaning, the FTO was quickly heated in a 180 °C blast dryer to vaporize the ethanol quickly. The FTO substrates were then placed in a UV ozone cleaner for 15 min. 1.25 g of urea (99.999%), 275 mg of SnCl$_2$·H$_2$O (99.99%) and 54 mg of TDGA (98%) were added to 100 mL of deionized water and stirred, and then 1.25 mL of concentrated hydrochloric acid was added after complete dissolution. The FTO substrate was immersed in the SnO$_2$ sol and deposited in a chemical bath in an oven at 180 °C for 3 h. After cooling to room temperature, ultrasonic cleaning was performed with deionized water and ethanol for 5 min respectively, and then drying was performed with blast drying oven. The OIHPs precursor solutions contained FAI (1.19 M), PbI$_2$ (1.31 M), MABr (0.21 M), PbBr$_2$ (0.21 M) and CsI (0.07 M) dissolved in DMF : DMSO = 4 : 1 (v : v).

PSCs fabricated using different methods

PSCs prepared without AS method. The OIHPs precursor solution was spin-coated on FTO/SnO$_2$ substrate, in a two-step procedure by spin coating at 1000 rpm for 10 s and 5000 rpm for 30 s respectively. During the second step, 150 μL chlorobenzene was poured on the spinning substrate 15 s before the end of the procedure. Next, the devices were annealed at 100 °C for 75 min. Then, the HTL was spin-coated on the OIHPs substrates at 3500 rpm for 30 s which was obtained by adding 72.3 mg of spiro-OMeTAD, 28.8 μL of 4-*tert*-butylpyridine, 17 μL of Li$^+$ salt, and 20 μL of cobalt(III) salt into 1 mL of chlorobenzene. Finally, the Au electrode was prepared by a high vacuum evaporation technology. The active area of the device was 0.15 cm^2, defined by the aperture area of the mask.

PSCs prepared with AS method. The OIHPs precursor solution was spin-coated on FTO/SnO$_2$ substrate, in a two-step

1476 | *Inorg. Chem. Front.,* 2024, **11**, 1472–1478

This journal is © the Partner Organisations 2024

procedure by spin coating at 1000 rpm for 10 s and 5000 rpm for 30 s respectively. During the second step, 150 μL ThMAI in chlorobenzene/isopropyl alcohol (v/v = 10 : 1) mixed solution was poured on the spinning substrate 15 s before the end of the procedure. After that, it was put back to the hot plate and thermally annealed at 100 °C for 75 min. The following steps were the same as those of PSCs prepared without AS method.

Post treatment modified PSCs. After the OIHPs film had cooled to room temperature, then apply 150 μL of ThMAI's isopropyl alcohol solution (0.05 mg mL^{-1}) to the top of OIHPs by spin coating at 4000 rpm for 30 s, annealing at 100 °C for 10 min. The following steps were the same as those of PSCs prepared without AS method.

Characterization

The cells were irradiated by Peccell-L15 solar simulator (Peccell, Japan) under AM 1.5G 100 mW cm^{-2}. Keithley 2460 (Keithley, America) was used to record the *J–V* characteristics of the cells. The test condition was that active area (0.15 cm^2 for PSCs) was defined by a black metallic mask, where scan rate was 0.2 V s^{-1} for both reverse and forward scan. Nyquist plot measurements were conducted with an electrochemical workstation (Zennium Zahner, Germany) under light illumination, under a 0.6 V forward bias voltages and with 20 mV amplitude of AC perturbation ranging from 100 mHz to 1 MHz. The obtained impedance spectra were fitted with the ZView software in terms of appropriate equivalent circuit model. The IPCE was performed employing a xenon lamp coupled with a monochromator (PEC-S20, Peccell) controlled by a computer. The morphology of different OIHPs films was observed by SEM (FEI Nova NanoSEM 450). The structure properties of OIHPs films were performed by XRD analysis (XRD-7000S, Shimadzu) from 2° to 65°. UV-vis absorbance spectra were measured by LAMBDA 950 (PerkinElmer, USA). PL spectra were obtained with a 517 nm laser using an optically triggered streak camera system (C5410, Hamamatsu). XPS was tested on Thermo Scientific, ESCLAB 250Xi, USA. The TPC/TPV and IMVS/IMPS measurements were conducted on the controlled intensity modulated photoelectric-chemical spectrometer of Zennium Zahner. The OIHPs films were tested for contact angle using a DataPhysics contact angle measuring instrument (OCAH200).

Author contributions

Chu Zhang: experiments, writing – original draft. Chunying Ma: data curation, formal analysis. Shennan Chen: formal analysis. Tingli Ma: funding acquisition, supervision, writing – review and editing.

Conflicts of interest

There are no conflicts to declare.

Acknowledgements

References

1 A. Kojima, K. Teshima, Y. Shirai and T. Miyasaka, Organometal Halide Perovskites as Visible-Light Sensitizers for Photovoltaic Cells, *J. Am. Chem. Soc.*, 2009, **131**, 6050–6051.

2 Z. Guo, A. K. Jena, G. M. Kim and T. Miyasaka, The high open-circuit voltage of perovskite solar cells: a review, *Energy Environ. Sci.*, 2022, **15**, 3171–3222.

3 W. Feng, J. Tao, G. Liu, G. Yang, J.-X. Zhong, Y. Fang, L. Gong, S. Yang and W.-Q. Wu, Near-Stoichiometric and Homogenized Perovskite Films for Solar Cells with Minimized Performance Variation, *Angew. Chem., Int. Ed.*, 2023, **62**, e202300265.

4 Z. Li, T. R. Klein, D. H. Kim, M. Yang, J. J. Berry, M. F. A. M. van Hest and K. Zhu, Scalable fabrication of perovskite solar cells, *Nat. Rev. Mater.*, 2018, **3**, 18017.

5 . Interactive Best Research-Cell Efficiency Chart., 2024.01.06, **https://www.nrel.gov/pv/cell-efficiency.html**.

6 K. X. Steirer, P. Schulz, G. Teeter, V. Stevanovic, M. Yang, K. Zhu and J. J. Berry, Defect Tolerance in Methylammonium Lead Triiodide Perovskite, *ACS Energy Lett.*, 2016, **1**, 360–366.

7 Z. Li, C. Xiao, Y. Yang, S. P. Harvey, D. H. Kim, J. A. Christians, M. Yang, P. Schulz, S. U. Nanayakkara, C.-S. Jiang, J. M. Luther, J. J. Berry, M. C. Beard, M. M. Al-Jassim and K. Zhu, Extrinsic ion migration in perovskite solar cells, *Energy Environ. Sci.*, 2017, **10**, 1234–1242.

8 J. Ye, M. M. Byranvand, C. O. Martínez, R. L. Z. Hoye, M. Saliba and L. Polavarapu, Defect Passivation in Lead-Halide Perovskite Nanocrystals and Thin Films: Toward Efficient LEDs and Solar Cells, *Angew. Chem., Int. Ed.*, 2021, **60**, 21636–21660.

9 M. I. Saidaminov, J. Kim, A. Jain, R. Quintero-Bermudez, H. Tan, G. Long, F. Tan, A. Johnston, Y. Zhao, O. Voznyy and E. H. Sargent, Suppression of atomic vacancies via incorporation of isovalent small ions to increase the stability of halide perovskite solar cells in ambient air, *Nat. Energy*, 2018, **3**, 648–654.

10 J. Park, J. Kim, H.-S. Yun, M. J. Paik, E. Noh, H. J. Mun, M. G. Kim, T. J. Shin and S. I. Seok, Controlled growth of perovskite layers with volatile alkylammonium chlorides, *Nature*, 2023, **616**, 724–730.

11 W. Zhao, Z. Yao, F. Yu, D. Yang and S. Liu, Alkali Metal Doping for Improved CH$_3$NH$_3$PbI$_3$ Perovskite Solar Cells, *Adv. Sci.*, 2018, **5**, 1700131.

12 X. Chang, J.-X. Zhong, S. Li, Q. Yao, Y. Fang, G. Yang, Y. Tan, Q. Xue, L. Qiu, Q. Wang, Y. Peng and W.-Q. Wu, Two-Second-Annealed 2D/3D Perovskite Films with Graded

This journal is © the Partner Organisations 2024

Inorg. Chem. Front., 2024, **11**, 1472–1478 | **1477**

Energy Funnels and Toughened Heterointerfaces for Efficient and Durable Solar Cells, *Angew. Chem., Int. Ed.*, 2023, **62**, e202309292.

13 H. Zhang, Y. Wu, C. Shen, E. Li, C. Yan, W. Zhang, H. Tian, L. Han and W.-H. Zhu, Efficient and Stable Chemical Passivation on Perovskite Surface via Bidentate Anchoring, *Adv. Energy Mater.*, 2019, **9**, 1803573.

14 B. Liu, M. Long, M. Cai, L. Ding and J. Yang, Interfacial charge behavior modulation in 2D/3D perovskite heterostructure for potential high-performance solar cells, *Nano Energy*, 2019, **59**, 715–720.

15 B. Chen, P. N. Rudd, S. Yang, Y. Yuan and J. Huang, Imperfections and their passivation in halide perovskite solar cells, *Chem. Soc. Rev.*, 2019, **48**, 3842–3867.

16 J. Xia, C. Liang, H. Gu, S. Mei, S. Li, N. Zhang, S. Chen, Y. Cai and G. Xing, Surface Passivation Toward Efficient and Stable Perovskite Solar Cells, *Energy Environ. Mater.*, 2023, **6**, e12296.

17 C. Sun, L. Xu, X. Lai, Z. Li and M. He, Advanced Strategies of Passivating Perovskite Defects for High-Performance Solar Cells, *Energy Environ. Mater.*, 2021, **4**, 293–301.

18 D.-Y. Son, S.-G. Kim, J.-Y. Seo, S.-H. Lee, H. Shin, D. Lee and N.-G. Park, Universal Approach toward Hysteresis-Free Perovskite Solar Cell via Defect Engineering, *J. Am. Chem. Soc.*, 2018, **140**, 1358–1364.

19 Y. Shao, Z. Xiao, C. Bi, Y. Yuan and J. Huang, Origin and elimination of photocurrent hysteresis by fullerene passivation in $CH_3NH_3PbI_3$ planar heterojunction solar cells, *Nat. Commun.*, 2014, **5**, 5784.

20 G. Yang, P. Qin, G. Fang and G. Li, A Lewis Base-Assisted Passivation Strategy Towards Highly Efficient and Stable Perovskite Solar Cells, *Sol. RRL*, 2018, **2**, 1800055.

21 X. Zheng, B. Chen, J. Dai, Y. Fang, Y. Bai, Y. Lin, H. Wei and C. Xiao, Zeng and J. Huang, Defect passivation in hybrid perovskite solar cells using quaternary ammonium halide anions and cations, *Nat. Energy*, 2017, **2**, 17102.

22 M. Li, X. Yan, Z. Kang, Y. Huan, Y. Li, R. Zhang and Y. Zhang, Hydrophobic Polystyrene Passivation Layer for Simultaneously Improved Efficiency and Stability in Perovskite Solar Cells, *ACS Appl. Mater. Interfaces*, 2018, **10**, 18787–18795.

23 D. Koushik, W. J. H. Verhees, Y. Kuang, S. Veenstra, D. Zhang, M. A. Verheijen, M. Creatore and R. E. I. Schropp, High-efficiency humidity-stable planar perovskite solar cells based on atomic layer architecture, *Energy Environ. Sci.*, 2017, **10**, 91–100.

24 M. A. Mahmud, T. Duong, Y. Yin, H. T. Pham, D. Walter, J. Peng, Y. Wu, L. Li, H. Shen, N. Wu, N. Mozaffari, G. Andersson, K. R. Catchpole, K. J. Weber and T. P. White, Double-Sided Surface Passivation of 3D Perovskite Film for High-Efficiency Mixed-Dimensional Perovskite Solar Cells, *Adv. Funct. Mater.*, 2020, **30**, 1907962.

25 H. Lu, Y. Liu, P. Ahlawat, A. Mishra, W. R. Tress, F. T. Eickemeyer, Y. Yang, F. Fu, Z. Wang, C. E. Avalos, B. I. Carlsen, A. Agarwalla, X. Zhang, X. Li, Y. Zhan, S. M. Zakeeruddin, L. Emsley, U. Rothlisberger, L. Zheng, A. Hagfeldt and M. Grätzel, Vapor-assisted deposition of highly efficient, stable black-phase $FAPbI_3$ perovskite solar cells, *Science*, 2020, **370**, eabb8985.

26 X. Jiang, S. Chen, Y. Li, L. Zhang, N. Shen, G. Zhang, J. Du, N. Fu and B. Xu, Direct Surface Passivation of Perovskite Film by 4-Fluorophenethylammonium Iodide toward Stable and Efficient Perovskite Solar Cells, *ACS Appl. Mater. Interfaces*, 2021, **13**, 2558–2565.

27 Y. Fang, T. Tian, M. Yang, Y. Tan, J.-X. Zhong, Y. Huang, X. Wang, J. Tao, S. Yang, C. Zou, S. Yang, Y. Peng, Q. Xue and W.-Q. Wu, Tailoring Pr ecursor Chemistry Enabled Room Temperature-Processed Perovskite Films in Ambient Air for Efficient and Stable Solar Cells with Improved Reproducibility, *Adv. Funct. Mater.*, 2023, **33**, 2303674.

28 X. Wang, J. Wu, Y. Yang, X. Liu, Q. Guo, Z. Song, G. Li, Z. Lan and M. Huang, High performance and stable perovskite solar cells using vanadic oxide as a dopant for spiro-OMeTAD, *J. Mater. Chem. A*, 2019, **7**, 13256–13264.

29 Q. Jiang, Y. Zhao, X. Zhang, X. Yang, Y. Chen, Z. Chu, Q. Ye, X. Li, Z. Yin and J. You, Surface passivation of perovskite film for efficient solar cells, *Nat. Photonics*, 2019, **13**, 460–466.

30 J. Chen, Y. Yang, H. Dong, J. Li, X. Zhu, J. Xu, F. Pan, F. Yuan, J. Dai, B. Jiao, X. Hou, A. K.-Y. Jen and Z. Wu, , Highly efficient and stable perovskite solar cells enabled by low-dimensional perovskitoids, *Sci. Adv.*, 2022, **8**, eabk2722.

1478 | *Inorg. Chem. Front.*, 2024, **11**, 1472–1478

This journal is © the Partner Organisations 2024